Draft version April 11, 2023
Typeset using LaTeX **twocolumn** style in AASTeX631

AST425 Final Paper
Constraining Cosmological Parameters with Gravitational Waves from Binary Black Hole Mergers

Lisa Nasu-Yu[1]

Maya Fishbach[1,2]
Supervisor

[1] *David A. Dunlap Department of Astronomy & Astrophysics, University of Toronto*
50 St. George Street
Toronto, Ontario, Canada M5S 3H4
[2] *Canadian Institute for Theoretical Astrophysics, University of Toronto*
60 St. George Street
Toronto, ON. M5S 3H8

ABSTRACT

We developed a new flexible statistical method using standard sirens to constrain the Hubble parameter. We applied our method to simulated gravitational-wave binary black hole events and forecast constraints on the Hubble constant. For mock black hole masses drawn from a mixture distribution with power law of slope -3.5 ranging from 5-80$M_\odot$ and 2 Gaussian peaks at $10M_\odot$ and $34M_\odot$, and cosmological parameters, H_0 =68km/s/Mpc, $\Omega_{m,0} = 0.3$, and $\Omega_{\Lambda,0} = 0.7$, our method found a Hubble constant of $67.3^{+4.0}_{-4.0}$km/s/Mpc, with 68% confidence, successfully placing the chosen $H_0 = 68$km/s/Mpc within uncertainties. Our method is also able to identify astrophysical evolution of features in the mass distribution with redshift. With the uncertainties in our model, we were able to identify a linear evolution to a precision of $0.05M_\odot$/Gpc.

1. INTRODUCTION

The expansion rate of the universe has been a focus in cosmology especially since the discovery of its acceleration in 1998 (Perlmutter et al. 1998; Riess et al. 1998). The Hubble parameter, $H(z)$, is a direct probe of the ΛCDM model, and constraining this function can inform the expansion history of the universe and the nature of dark energy.

However, values of the Hubble parameter today, known as the Hubble constant, H_0, obtained through local measurements such as standard candles (Riess et al. 2022) disagree with that of early universe CMB studies by (Planck Collaboration et al. 2020); a contradiction known as the Hubble tension. Furthermore, the nature of dark energy remains unknown. In efforts to solve this problem, researchers are searching for ways to improve constraints on the Hubble parameter, or uncover new physics that may allow for the discrepancy in early versus late universe values of the Hubble parameter.

With the increasing range and precision of gravitational wave (GW) detection in the recent decade, a GW analog to standard candles has come to focus – the standard siren. Merging black holes and neutron stars are strong sources of gravitational waves and serve as standard sirens. For standard sirens, the luminosity distance, D_L, and redshifted chirp mass, $\mathcal{M}_z = \mathcal{M}(1+z)$, of the source can be obtained directly from the gravitational waves, where the chirp mass, $\mathcal{M}$, is an effective mass of the binary system with the form,

$$\mathcal{M} = \frac{(m_1 m_2)^{3/5}}{(m_1 + m_2)^{1/5}}. \quad (1)$$

Standard sirens are especially powerful because they are self calibrating and can probe the universe at cosmological scales of $z > 1$ and $D_L > 5$Gpc (Schutz 1986; Holz & Hughes 2005). Unlike standard candles which require a distance ladder to determine the source distance, the luminosity distance from standard sirens is directly encoded in the GW based on the theory of general relativity. As such, standard sirens minimize the uncertainty on luminosity distance to just noise and instrument error. Since the luminosity distance is directly derived from general relativity, standard sirens can also be used as a test for gravity.

Given the luminosity distance, the remaining challenge is to determine the corresponding redshift. With these 2 values, we can use the luminosity distance equation (Equation 2) to infer values on the local expansion rate of the universe, as well as the composition of the universe through the ΛCDM model.

$$D_L = c(1+z)\int_0^z \frac{dz'}{H_0 E(z')} \tag{2}$$

Then, with H_0 calculated as above, we can constrain the Hubble parameter at all redshifts,

$$H(z) = H_0\sqrt{E(z)}. \tag{3}$$

Currently existing standard siren methods to constrain the expansion of the universe include bright sirens, which require an electromagnetic (EM) counterpart to the merger, and dark sirens, which do not require an EM counterpart (e.g. Moresco et al. 2022).

For bright sirens, the EM counterpart is used to uniquely identify the merger's host galaxy, from which the redshift is obtained. However, to date, there has been only one detection of a standard siren with an EM counterpart – GW170817, a binary neutron star merger detected in 2017. This analysis presented an H_0 of $70^{+12.0}_{-8.0}$km/s/Mpc (Abbott et al. 2017). To further constrain the Hubble constant with this method, many more GW detections with EM counterparts would be required.

We have many GW detections without EM counterparts, numbering at around 100 mergers. However, GW detections are difficult to localize on the sky, usually preventing the unique identification of a host galaxy. Where a complete galaxy survey is available, the galaxy catalog dark siren method estimates z by statistically marginalizing over all potential host galaxies within the localization volume of the detected merger, but presents greater uncertainties than bright sirens with their unique host galaxy identification.

Another approach, known as spectral sirens, uses information about neutron star or black hole mass distribution to infer cosmology without the need for counterparts or galaxy catalogs (Taylor et al. 2012; Farr et al. 2019).

In this study, we developed a flexible statistical technique for spectral siren cosmology, independent of the rare detection of EM counterparts or the localization of the merger, to determine a z–D_L relation to constrain the Hubble parameter.

2. METHODS

In the information encoded in gravitational waves, there is a perfect degeneracy between the chirp mass and redshift. As we require z to infer H_0 from Equation 2, the purpose of this study was to develop robust statistical techniques to disentangle $\mathcal{M}$ and z.

There is expected to be no general correlation between a black hole's true mass and its luminosity distance; however, the detected redshifted mass ($\mathcal{M}_z$) increases with D_L, as the gravitational waves encoding the mass undergo cosmological redshift. This cosmological redshift is reflected in our simulation of BBH merger chirp mass and luminosity distance distributions in Figure 1.

Our simulation focused on BBH mergers, assuming binary black holes of equal mass ratios; an appropriate assumption at this stage as inferences from the Gravitational Wave Transient Catalogue (GWTC)-3 showed the mass ratio to be modeled by a power law of slope $\beta = 1.1^{+1.7}_{-1.3}$(The LIGO Scientific Collaboration et al. 2021), favoring equal mass ratios. We also approximated the merger rate to be uniform in Euclidean volume, making our luminosity distance distribution proportional to D_L^3.

Our initial source-frame mass distribution used simple parameters based from GWTC-3 for a mass mixture distribution of 95% power law with slope -3.5 ranging from a primary mass of 5-80$M_\odot$ and 5% Gaussian with a peak at 34$M_\odot$ and standard deviation of 2$M_\odot$. For this initial simulated mass distribution, we assumed that source frame masses, specifically the location of the Gaussian peak, do not depend on redshift.

We simulated a population of 10,000 black hole mergers from the above luminosity distance and mass distributions, then applied redshift to the mass sample, calculated with Equation 2 for H_0 =68km/s/Mpc and $\Omega_{m,0} = 0.3$, as shown in Fig. 1. We constrained H_0 in our model by statistically determining a z–D_L relation that best removed the $\mathcal{M}_z - D_L$ correlation, assuming that source-frame masses and distances are not correlated.

In order to find the peak in chirp mass, we first used a Gaussian kernel density estimation (KDE) of bandwidth 0.5 to map overdensities in the joint $\mathcal{M}_z$–D_L distribution. We then found contours of the peaks in the $\mathcal{M}_z$ component using the partial and second partial derivatives of the KDE along the $\mathcal{M}_z$ component, with resolution of 0.05 in log space. We computed the running mean of the contours to minimize statistical fluctuations in the contours. We then distinguished overdensities due to Poisson noise statistics from the power law component from the astrophysical features in the mass distribution. We extracted only overdensities associated with an astrophysical feature (Gaussian peak) by filtering for on average increasing contours spanning at least 12Gpc. These filter choices were made as we expect any astro-

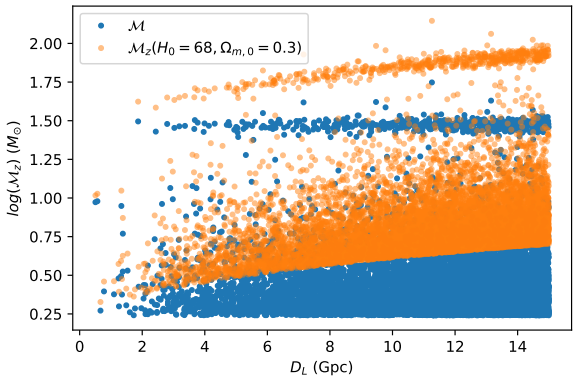

Figure 1. Chirp mass, $\mathcal{M}$, and redshifted chirp mass, $\mathcal{M}_z$, for 10000 black hole mergers simulated from a mass mixture distribution of 95% power law with slope -3.5 ranging from a primary mass of 5-80$M_\odot$ and 5% Gaussian with a peak at 34$M_\odot$ and standard deviation of 2$M_\odot$, and cosmological parameters H_0=68km/s/Mpc, $\Omega_{m,0}$=0.3, and $\Omega_{\Lambda,0}$=0.7.

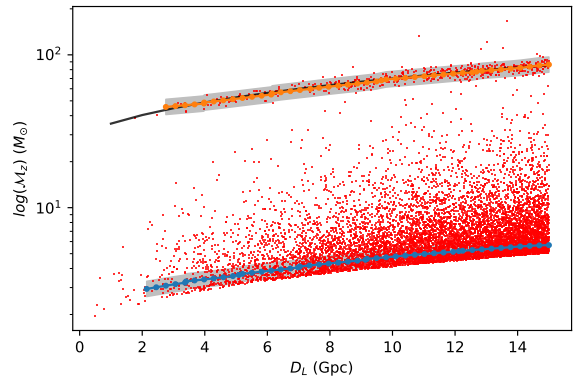

Figure 2. In red is the BBH merger sample population. Dotted curves show local maxima contours in BBH overdensities, extracted after filtering. Shaded gray represents a band of width 0.05 in log space, indicating the region within which sample points were included in the linear fit to evaluate H_0. The black curve represents the expected peak at primary mass 34$M_\odot$, showing that it was successfully retrieved by the orange dotted curve. The second contour in blue is picking up the power law cutoff at 5$M_\odot$.

physical feature to be apparent across a large range in distance, and a mass-distance correlation due to cosmological redshift should result in an increasing correlation between $\mathcal{M}_z$ and D_L.

We used all data points within 0.05 in log space (corresponding to the resolution of the KDE derivatives computed) of the extracted contour in our further fitting analysis. For various values of H_0, we computed the corresponding z for each eligible sample point, retrieved the hypothetical source-frame mass for such H_0, $\mathcal{M} = \mathcal{M}_z/(z+1)$, and applied a linear fit. We expect values close the the true H_0 to result in a horizontal $\mathcal{M}$–D_L line. The value of H_0 that minimized the magnitude of the slope in the linear fit was determined to be the best fit. We evaluated the best fit H_0 for each feature picked up in the overdensity-finding algorithmm but focus on the 34$M_\odot$ astrophysical feature. We used this method and bootstrapping of the sample points to determine a constraint on H_0 of $69.7^{+7.1}_{-3.3}$km/s/Mpc (68% confidence level).

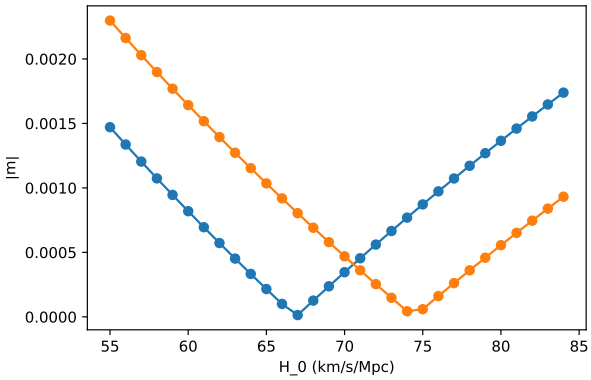

Figure 3. Magnitude of slopes, m, from linear fits to the "unredshift" source frame $\mathcal{M}$–D_L points, given Hubble constants ranging from 55 to 85 km/s/Mpc in the 1 feature model. For this iteration, our method presented 67km/s/Mpc and 74km/s/Mpc as having the slope closest to zero, and thus the best fit, for the power law cutoff (blue) and Gaussian peak (orange).

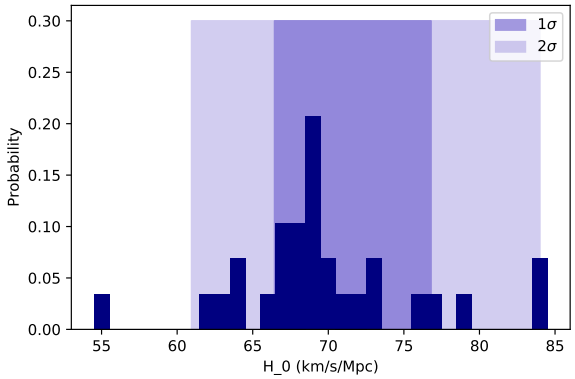

Figure 4. Probability of values for best fit Hubble constants for 50 iterations of resampling 10000 points from the original 1-feature simulated sample. Dark and light blue shading shows 68% and 95% confidence levels, resulting in $H_0 = 69.7^{+7.1}_{-3.3}$km/s/Mpc and $H_0 = 69.7^{+14.3}_{-8.8}$km/s/Mpc, respectively.

We tested the effect our choice of sample size has on the result. Repeating our method on the same population with 5000 and 20000 resampled points resulted in $H_0 = 66.9^{+9.2}_{-10.8}$±km/s/Mpc and $H_0 = 71.2^{+5.4}_{-4.8}$±km/s/Mpc to 1σ uncertainties, respectively, showing an increase in resampling size tightens our uncertainties.

3. RESULTS

To better represent the BBH population inferred from GWTC-3 (The LIGO Scientific Collaboration et al. 2021), we applied our method to the original mass mixture model with an additional Gaussian peak at $10M_\odot$, again with a standard deviation of $2M_\odot$. Repeating the method described above, we obtain 2 constraints on H_0, from fitting each peak. We evaluated $H_0 = 67.4^{+6.9}_{-11.2}$km/s/Mpc from the $10M_\odot$ peak, and $H_0 = 67.3^{+4.0}_{-4.0}$km/s/Mpc from the $34M_\odot$ peak for 68% confidence levels. The $10M_\odot$ peak is poorly constrained because, being a lower mass, it was harder to distinguish from the underlying power law continuum. However, both these values are in agreement with the known Hubble constant of 68km/s/Mpc in this model.

In addition to the cosmological redshift, we expect to see some evolution of the mass distribution depending on astrophysical conditions during black hole original star formation, such as metallicity. The abundance of metals in the universe increases with age through processes such as nuclear fusion and ejection through stellar winds in stars and r-processes in supernovae. The shape of this mass evolution is not well understood, but is expected to increase with redshift due to the increasing metallicity in its progenitor stars. We can use our method to identify astrophysical evolution by comparing the luminosity distance correlation of each feature in the mass distribution. As a toy model, we tested our method with a linear evolution,

$$M_z = 10(1+z) + mD_L, \tag{4}$$

in the $10M_\odot$ Gaussian peak of the previous 2 feature model, with varying slope, m.

Although we do not obtain good constraints from the non-evolving $10M_\odot$ peak (Figure 6), it it is able to clearly distinguish between the evolving and non-evolving cases. The evolving plot shows all 50 resampling iterations with unrealistically far H_0's from our expected value of 68km/s/Mpc, indicating the existence of astrophysical evolution in this feature.

We determined constraints on H_0 from the $34M_\odot$ peak, then used this value to infer the evolution in the $10M_\odot$ peak. The $34M_\odot$ peak suggested an H_0 of $67.3^{+4.0}_{-4.0}$km/s/Mpc. Taking this to be H_0 for our model,

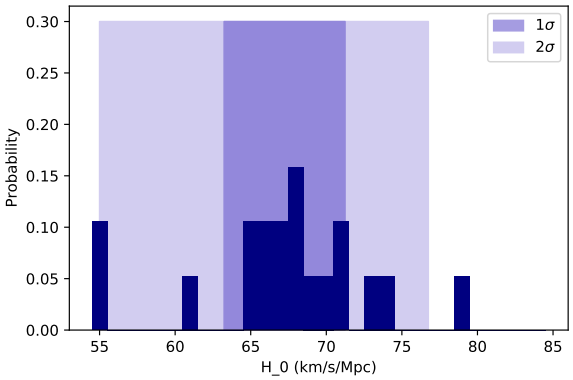

Figure 5. Probability for values of best fit Hubble constant from the $34M_\odot$ feature for 50 iterations of resampling from the 2 feature model. We obtained $H_0 = 67.3^{+4.0}_{-4.0}$km/s/Mpc and $H_0 = 67.3^{+9.5}_{-12.3}$km/s/Mpc for 68% and 95% confidence levels, respectively.

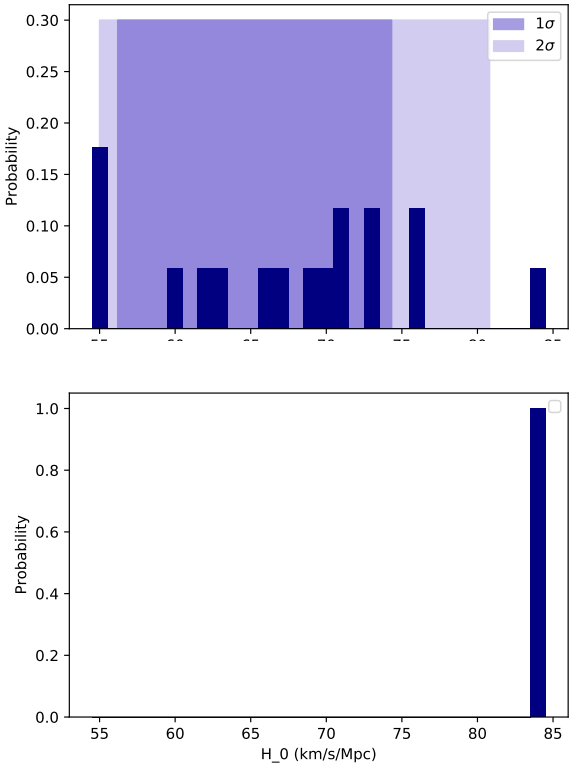

Figure 6. Probability for values of best fit Hubble constant from the non-evolving $10M_\odot$ peak (top) and evolving $10M_\odot$ peak (bottom) for 50 iterations of resampling 10000 points from the simulated sample population. The mass distribution of the evolving feature was based on the non-evolving feature, with an additional linear shift to represent astrophysical evolution with z.

dividing this from the slope of the $10M_\odot$ peak in the

previous linear fit leaves behind only the evolution, as shown in Equation 4.

Given a linear evolution with slope $m = 0.5 M_\odot$/Gpc, we retrieved a slope of $m = 0.49^{+0.02}_{-0.05} M_\odot$/Gpc with 68% confidence, placing the true slope within errors.

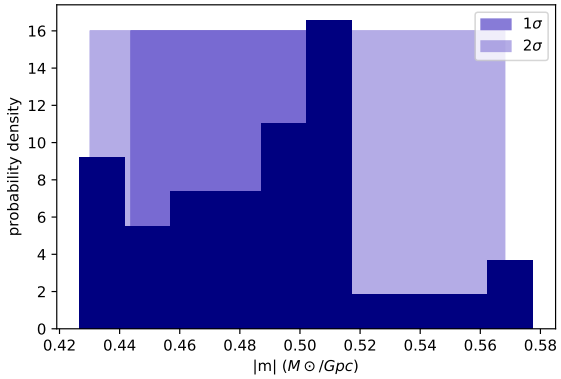

Figure 7. Probability of linear astrophysical evolution slope from 50 resampling iterations, evaluated using our calculated H_0 of 67.3km/s/Mpc. Dark and light blue shading show 68% and 95% confidence levels of the mean slope, respectively.

Astrophysical evolution is difficult to determine simultaneously with cosmology, especially for small and/or complicated evolutions as it is degenerate with the cosmological redshift. With our uncertainties in H_0, the smallest slope for the linear evolution we were able to successfully infer was 0.05 $M_\odot$/ Gpc.

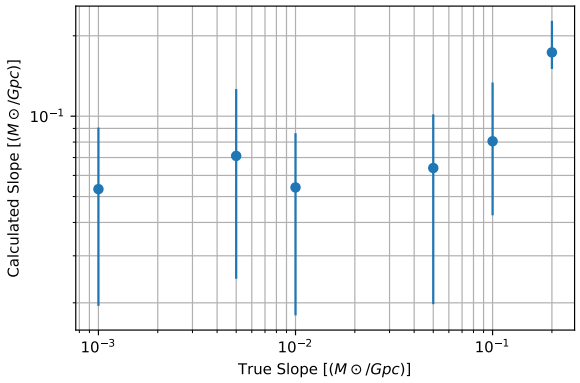

Figure 8. Best fit slopes evaluated from linear astrophysical evolution, compared to the true underlying slope. Error bars show 68% confidence levels. 0.05 $M_\odot/Gpc$ was the minimum slope that our method was able to successfully extract.

4. DISCUSSION

Further development of this statistical technique will allow the forecasting of expected constraints on $H(z)$ for more complicated, realistic mass distributions.

With around 100 GW detections today, there is not enough data to apply this method directly to real data. However, in the coming decades, upcoming next generation GW detectors, such as the Einstein Telescope, Cosmic Explorer, and LISA, are anticipated to usher in an era of precision cosmology with gravitational waves. GW detections are expected to number in the hundreds of thousands, allowing future studies to be able to apply this technique directly to data to constrain cosmological parameters.

A remaining challenge in this method is separating overdense peaks from the underlying power law continuum in the mass distribution. While we obtained constraints on H_0 from the $34 M_\odot$ peak, we were unable to adequately constrain H_0 using the $10 M_\odot$ peak, which, being at a lower mass, was harder to distinguish from the underlying power law continuum.

This statistical method is unique in that it is able to simultaneously infer astrophysical evolution and cosmological redshift for arbitrary mass distributions. The identification of astrophysical features is dependent on analysing detected overdensities in the population and it is not prone to biases from our incomplete understanding of the mass distribution, unlike commonly-used, parametric fits.

While we focused on a monotonic linear evolution, future work includes testing this method with various forms of evolution. We considered the effects of star metallicity to decide on a monotic linear evolution for this study, but other factors including delay time and environment (such as globular clusters) may cause different forms of evolution.

Applying this technique to real data in the future will identify overdense astrophysical peaks and may inform us on previously unknown features in the mass distribution, furthering our understanding of black hole populations and their progenitor stars.

5. CONCLUSION

From our simulation with H_0=68km/s/Mpc, and 2 Gaussian peaks in the mass distribution at $10 M_\odot$ and $34 M_\odot$, our method inferred a Hubble constant of $67.3^{+4.0}_{-4.0}$km/s/Mpc to 68% confidence, placing the true value within errors. This method was able to identify linear astrophysical evolution in the same model to a resolution of $0.05 M_\odot$/Gpc.

REFERENCES

Abbott, B., Abbott, R., Abbott, T., et al. 2017, Physical Review Letters, 119, doi: 10.1103/physrevlett.119.161101

Farr, W. M., Fishbach, M., Ye, J., & Holz, D. E. 2019, The Astrophysical Journal, 883, L42, doi: 10.3847/2041-8213/ab4284

Holz, D. E., & Hughes, S. A. 2005, The Astrophysical Journal, 629, 15, doi: 10.1086/431341

Moresco, M., Amati, L., Amendola, L., et al. 2022, Unveiling the Universe with Emerging Cosmological Probes, arXiv, doi: 10.48550/ARXIV.2201.07241

Perlmutter, S., Aldering, G., Deustua, S., et al. 1998, doi: 10.48550/ARXIV.ASTRO-PH/9812473

Planck Collaboration, Aghanim, N., Akrami, Y., et al. 2020, Astronomy & Astrophysics, 641, A6, doi: 10.1051/0004-6361/201833910

Riess, A. G., Filippenko, A. V., Challis, P., et al. 1998, The Astronomical Journal, 116, 1009, doi: 10.1086/300499

Riess, A. G., Yuan, W., Macri, L. M., et al. 2022, The Astrophysical Journal Letters, 934, L7, doi: 10.3847/2041-8213/ac5c5b

Schutz, B. F. 1986, Nature, 323, 310, doi: 10.1038/323310a0

Taylor, S. R., Gair, J. R., & Mandel, I. 2012, Physical Review D, 85, doi: 10.1103/physrevd.85.023535

The LIGO Scientific Collaboration, The Virgo Collaboration, The KAGRA Collaboration, et al. 2021, doi: 10.48550/ARXIV.2111.03634